NREL
NATIONAL RENEWABLE ENERGY LABORATORY

The Effects of Second-Order Hydrodynamics on a Semisubmersible Floating Offshore Wind Turbine

Preprint

I. Bayati
Politecnico di Milano

J. Jonkman, A. Robertson, and A. Platt
National Renewable Energy Laboratory

Presented at the Science of Making Torque from Wind
Technical University of Denmark, Copenhagen
June 17–20, 2014

NREL is a national laboratory of the U.S. Department of Energy
Office of Energy Efficiency & Renewable Energy
Operated by the Alliance for Sustainable Energy, LLC

This report is available at no cost from the National Renewable Energy Laboratory (NREL) at www.nrel.gov/publications.

Conference Paper
NREL/CP-5000-61752
July 2014

Contract No. DE-AC36-08GO28308

NOTICE

This report is available at no cost from the National Renewable Energy Laboratory (NREL) at www.nrel.gov/publications.

Available electronically at http://www.osti.gov/scitech

Available for a processing fee to U.S. Department of Energy and its contractors, in paper, from:

U.S. Department of Energy
Office of Scientific and Technical Information
P.O. Box 62
Oak Ridge, TN 37831-0062
phone: 865.576.8401
fax: 865.576.5728
email: mailto:reports@adonis.osti.gov

Available for sale to the public, in paper, from:

U.S. Department of Commerce
National Technical Information Service
5285 Port Royal Road
Springfield, VA 22161
phone: 800.553.6847
fax: 703.605.6900
email: orders@ntis.fedworld.gov
online ordering: http://www.ntis.gov/help/ordermethods.aspx

Cover Photos: (left to right) photo by Pat Corkery, NREL 16416, photo from SunEdison, NREL 17423, photo by Pat Corkery, NREL 16560, photo by Dennis Schroeder, NREL 17613, photo by Dean Armstrong, NREL 17436, photo by Pat Corkery, NREL 17721.

The effects of second-order hydrodynamics on a semisubmersible floating offshore wind turbine

I Bayati[1], J Jonkman[2], A Robertson[2] and A Platt[2]

[1] Politecnico di Milano, Dipartimento di Meccanica, Milano, Italy
[2] National Renewable Energy Laboratory (NREL), Golden, CO, USA
E-mail: ilmasandrea.bayati@polimi.it, jason.jonkman@nrel.gov, amy.robertson@nrel.gov, andrew.platt@nrel.gov

Abstract. The objective of this paper is to assess the second-order hydrodynamic effects on a semisubmersible floating offshore wind turbine. Second-order hydrodynamics induce loads and motions at the sum- and difference-frequencies of the incident waves. These effects have often been ignored in offshore wind analysis, under the assumption that they are significantly smaller than first-order effects. The sum- and difference-frequency loads can, however, excite eigenfrequencies of a floating system, leading to large oscillations that strain the mooring system or vibrations that cause fatigue damage to the structure. Observations of supposed second-order responses in wave-tank tests performed by the DeepCwind consortium at the Maritime Research Institute Netherlands (MARIN) offshore basin suggest that these effects might be more important than originally expected. These observations inspired interest in investigating how second-order excitation affects floating offshore wind turbines and whether second-order hydrodynamics should be included in offshore wind simulation tools like FAST. In this work, the effects of second-order hydrodynamics on a floating semisubmersible offshore wind turbine are investigated. Because FAST is currently unable to account for second-order effects, a method to assess these effects was applied in which linearized properties of the floating wind system derived from FAST (including the 6x6 mass and stiffness matrices) are used by WAMIT to solve the first- and second-order hydrodynamics problems in the frequency domain. The method was applied to the Offshore Code Comparison Collaboration Continuation (OC4)-DeepCwind semisubmersible platform, supporting the National Renewable Energy Laboratory's 5-MW baseline wind turbine. In this paper, the loads and response of the system caused by the second-order hydrodynamics are analyzed and compared to the first-order hydrodynamic loads and induced motions in the frequency domain. Further, the second-order loads and induced response data are compared to the loads and motions induced by aerodynamic loading as solved by FAST.

1. Introduction

Nowadays offshore wind energy is moving to deeper waters, where floating platforms seem to be the most suitable solution. This paper aims to assess the effects of second-order hydrodynamics on the overall dynamics of a semisubmersible platform combined with the National Renewable Energy Laboratory's (NREL's) 5-MW reference wind turbine [1].

Presently, most aero-hydro-servo-elastic simulation tools used for designing floating offshore wind turbines include only first-order hydrodynamics, which induce loads and motions that vary with the same frequency as the incident waves; however, the offshore oil and gas industry has demonstrated the importance of second-order hydrodynamics—solved either directly or with Newman's approximation [2] on floating system design. Second-order hydrodynamics can induce loads at the sum- and difference-frequencies of the incident wave components, which can excite eigenfrequencies of the system, leading to large oscillations that strain the mooring system or

vibrations that cause fatigue damage to the structure. A recent study assessed the importance of second-order hydrodynamics on the Offshore Code Comparison Collaboration (OC3)-Hywind spar buoy and University of Maine tension-leg platform (TLP) floating offshore wind turbine (FOWT) concepts [3]. In this paper, the approach defined in [3] was applied to analyze the semisubmersible platform designed by the University of Maine and used within the International Energy Agency (IEA) Wind Task 30 Offshore Code Comparison Collaboration Continuation (OC4) project, shown in figure 1 [4]. A $1/50^{th}$ Froude-scaled model of this system was tested in a wind/wave basin at the Maritime Research Institute Netherlands (MARIN) in 2011 [5] by the DeepCwind consortium. Validation of a FAST model using this test data showed evidence of the importance of considering second-order hydrodynamics; particularly, second-order difference-frequency wave-diffraction loading played a significant role in the global response of the floating semisubmersible system because the surge, pitch, and heave natural frequencies are lower than the wave-frequency band. The low-frequency wind energy from atmospheric turbulence also excites the wind turbine in the same frequency band. The wind forcing and first-order hydrodynamic loading is captured by FAST, but neglecting the second-order hydrodynamics inevitably underestimates the global response.

2. Second-order hydrodynamics

Potential flow theory considers the flow around a body to be incompressible, inviscid, and irrotational, with negligible surface-tension effects. The kinematics of the problem is typically described by a global coordinate system (GCS) that is located in an inertial frame of reference and assumed to be a right-handed Cartesian system with its origin located at the still water level. A second body-fixed coordinate system (BCS) that moves with the body has its axis coincident with the GCS when the body is in an undisturbed (mean) position. First-order theory for potential flow assumes a linear free-surface boundary condition and ignores nonlinear wave-body interaction effects. The first-order velocity potential is solved about the mean position of the body and the total hydrodynamic problem is solved by means of superposition of the independent solutions of subproblems, such that the radiation (i.e., the problem of the interactions caused by forced motions of the body in calm water), diffraction (i.e., the problem of the interactions of the incident waves with the body held fixed), and hydrostatic problems (i.e., the problem of buoyancy change with body displacement) can be solved independently. This superposition approach is valid mainly for a floating system with small translational displacements compared to the wave length and small rotations with respect to the wave steepness. Second-order hydrodynamic theory more accurately approximates the nonlinear free-surface boundary condition and wave-body interactions, including the quadratic interaction of first-order quantities. These hydrodynamics are computed by means of the superposition of the quadratic interaction of terms related to the first-order velocity potential, as well as terms given by the solution of the second-order velocity potential. The latter is derived by second-order Taylor expansion of the velocity potential, along with the expansion of the motion amplitude and wave elevation. Therefore, the velocity potential boundary value problem of the moving body is reformulated and solved with respect to a GCS.

The hydrodynamic forces and moments that result from the interaction of the fluid with a floating structure are obtained through the integration of the fluid pressure over the instantaneous wetted surface of the structure. Both first- and second-order approaches approximate this computation over the mean wetted profile of the floating structure; however, the assumption of inviscid flow limits the amount of hydrodynamic damping considered, requiring the potential-flow solution to be augmented with viscous effects where important. This augmentation is typically done by increasing the potential-flow solution with the viscous drag term from Morison's equation in a time-domain analysis to perform a more realistic simulation of the actual dynamics of such systems, as discussed in [6], [7].

Second-order hydrodynamic loads are proportional to the square of the wave amplitude and have frequencies that are equal to both the sum and the difference of pairs of incident wave frequencies. This means that, although the natural frequencies of the structure are designed to be outside the first-order wave-energy spectrum, the second-order loads can excite these frequencies. Therefore, despite the second-order hydrodynamic loads normally being small in magnitude, the resonant effect can be significant.

Three components of second-order hydrodynamic loads can be defined: the mean-drift loads, the difference-frequency/slow-varying drift loads, and the sum-frequency loads. The mean-drift loads result in a mean offset of the body relative to its undisplaced position. The slow-varying loads are the result of quadratic interactions between separate wave components in an irregular sea state that have different frequencies. These loads can excite large amplitude resonant motion of the floating platform at low frequency. The sum-frequency loads have a frequency that is higher than the wave frequency and are also generally small in amplitude. They arise from the same source as low-frequency drift forces, that is, from quadratic interactions between separate wave components in an irregular sea state. The contribution from these loads can be particularly important in relation to a "springing" and "ringing" phenomenon for floating wind turbine configurations with taut moorings, such as TLP concepts that typically have

high natural frequencies in heave, roll, and pitch. The sum-frequency second-order loads can also potentially excite vibration modes of the wind turbine [8].

The focus of this paper is to investigate the influence of second-order hydrodynamics on the OC4-DeepCwind floating semisubmersible system. Model validation work previously performed with this system using the MARIN tank data adopted Newman's slow-varying load approximation [5]. According to this approximation [2], the off-diagonal components of the difference-frequency quadratic transfer functions (QTFs) can be approximated by manipulating the diagonal values. Newman's approximation is valid when the natural frequencies of slowly varying motions are small, as in the present case. Nevertheless, this approximation may not be very reliable in shallow water, broad-banded sea states, or sea states with wave direction spreading. In the validation work of [5], a custom FAST tool was implemented using the second-order wave diffraction forces from Newman's approximation associated with the surge degree of freedom (DOF). In this paper, however, the unapproximated second-order loads were computed by WAMIT for all six DOFs [9].

3. Simulation tools and approach

To investigate the impact of second-order effects on the OC4-DeepCwind floating semisubmersible system, a combined modeling approach that incorporates WAMIT and FAST was used. In this section, the method will be explained, as it differs from the direct use of FAST in its present form. The two simulation tools used to assess the second-order effects in this work are FAST and WAMIT. FAST is a publicly available wind turbine simulation tool developed by NREL [6], [10] that predicts the coupled dynamic response of the entire FOWT in the time domain, thereby taking aerodynamics, structural elasticity, control logic, and first-order hydrodynamics plus viscous effects into account. WAMIT is a commercial, three-dimensional panel code designed to compute the hydrodynamic loading and response of floating bodies in the frequency domain [9], including first-order wave-exciting loads and response amplitude operators (RAOs), as well as the second-order load and response QTFs. WAMIT is widely used in the offshore industry and is capable of solving both the first- and second-order hydrodynamic problems for a rigid structure of arbitrary geometry. Currently, the coupled response of FOWTs simulated in FAST considers only first-order hydrodynamic quantities computed by WAMIT or an equivalent pre-processor. As a result, the procedure employed in this work to assess second-order hydrodynamics effects uses the approach developed in [3] that is briefly summarized below (shown in figure 2).

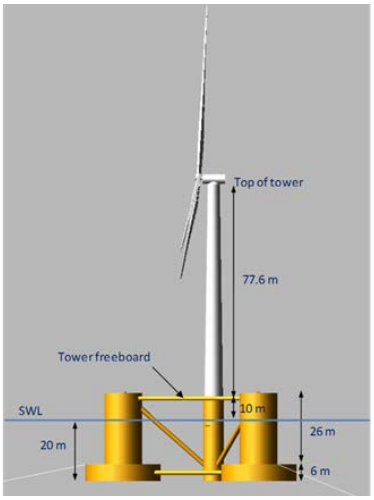

Figure 1. OC4-DeepCwind semisubmersible.

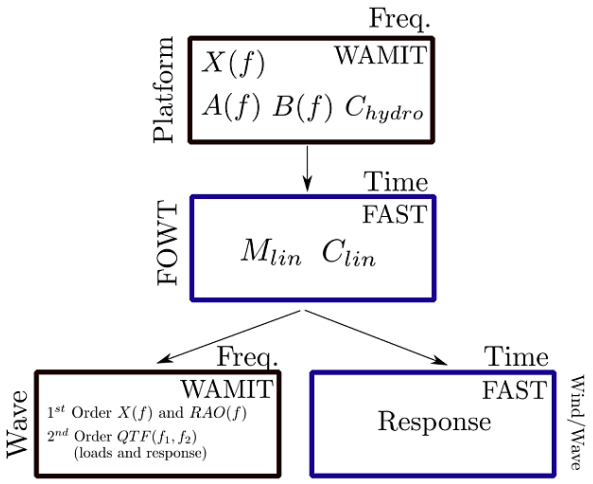

Figure 2. Procedure to assess first- and second-order hydrodynamics of the OC4 semisubmersible FOWT.

First, WAMIT was used to calculate the hydrostatic restoring (C_{hydro}), frequency-dependent hydrodynamic added mass and damping matrices from wave radiation ($A(f)$ and $B(f)$), and the frequency- and direction-dependent hydrodynamic force coefficients from wave diffraction ($X(f)$). These quantities are WAMIT outputs, based on the geometry of the submerged portion of the floating platform. It must also be stated that the investigation of the effect of a multidirectional sea state is beyond the aim of this work, therefore only one heading angle $\boldsymbol{\beta}=0$ on which the velocity potential is dependent was considered in the computations reported in this paper. In addition, the wind was aligned with the waves with no yaw misalignment. Second, the hydrodynamic quantities were given as inputs to FAST, together with inputs related to the wind turbine, floating platform, and mooring system specifications. The

FAST model was then used to compute the 6x6 mass matrix of the entire wind system (M_{lin}) and the 6x6 stiffness matrix of the mooring system (C_{lin}) through a linearization procedure. Being careful to avoid double-booking terms, these quantities were imported back into WAMIT as external matrices for the third step—calculating the first- and second-order frequency-dependent loads and responses (RAOs and QTFs), considering the properties of the entire system.

The natural frequencies of the OC4-DeepCwind semisubmersible platform were designed to fall below the wave-frequency range. Although viscous drag will tend to dominate the potential damping at these low frequencies, the first- and second-order WAMIT solutions were not augmented with linearized viscous effects. Nevertheless, as reported in [4] and [5], linear and quadratic damping is included in FAST for performing more realistic time-domain simulations. An important limitation to the calculation in WAMIT is that the structure is modelled as a rigid body, whereas FAST can model the structural elasticity. It should also be noted that wind turbine operational effects, such as rotor gyroscopics, aerodynamic damping, and aerodynamic stiffness, were ignored in the linearized matrices imported to WAMIT.

FAST is currently not configured to utilize the second-order force QTFs calculated by WAMIT. Therefore, the assessment summarized in this paper was conducted outside of FAST and within WAMIT only, by using FAST merely for generating the linearized matrices mentioned above and to perform simulations to compute the global response caused by the wind-wave and wave-only first-order hydrodynamic loads. The comparison between WAMIT and FAST was then possible by converting FAST's time-domain outputs to the frequency domain.

Regarding the WAMIT computations, the platform of figure 1 was discretized by a means of 1167 panels and a range of 56 wave frequencies in the interval [0.25 3.0] rad/s, with a frequency step of 0.05 rad/s using a high-order panel method. In the high-order computational approach, the potential on the body surface is represented by B-splines in both the first- and second-order analyses. In the first-order analysis, the forcing on the body surface is assumed continuous and the integration is carried out by Gauss quadrature. In the second-order analysis, however, the integration of the quadratic forcing on the body and the free surface is performed piecewise in the same manner as for the low-order analysis.

4. Post processing and results

In this section, the hydrodynamic loads and response of the floating semisubmersible (using the approach described above) are analyzed by considering the following DOFs: surge, pitch, and heave. These DOFs have associated natural frequencies of 0.01 Hz, 0.04 Hz, and 0.055 Hz, respectively. Figures 3, 4, and 5 show the first-order hydrodynamics solutions in terms of wave exciting loads $X(f) = |X(f)|e^{i\varphi_x}$ and motion response amplitude operators $RAO(f) = |RAO(f)|e^{i\varphi_{RAO}}$, whose magnitudes are provided by WAMIT as normalized per unit wave height, for a water depth of 200 m. The variation of load magnitude across the frequencies is a result of the interaction of the waves with the three distinct columns of the OC4-DeepCwind floating semisubmersible system; the natural frequencies are clearly visible in the RAOs. The very high magnitude corresponding to these frequencies is consistent with the lack of a significant damping in the model.

Similar to the first-order analysis, the second-order WAMIT outputs are normalized by pairs of incident wave amplitudes, so that it is possible to define the complex second-order loads ${F_{jk}}^{\pm} = \left|{F_{jk}}^{\pm}\right| e^{i{\varphi_{jk}}^{\pm}}$ and responses ${\xi_{jk}}^{\pm} = \left|{\xi_{jk}}^{\pm}\right| e^{i{\varphi_{jk}}^{\pm}}$, where $\left|{F_{jk}}^{\pm}\right|$ and $\left|{\xi_{jk}}^{\pm}\right|$ are the load and motion QTF magnitudes per square unit wave amplitude with phase ${\varphi_{jk}}^{\pm}$ that are associated with the complex wave-amplitude pairs, ${A_j}^{\pm} = \left|A_j\right| e^{i\varphi_j}$ and ${A_k}^{\pm} = |A_k| e^{i\varphi_k}$, at frequencies f_j and f_k, with the related random phases φ_j and φ_k, respectively. The magnitudes of the difference-frequency components of the second-order load and response QTFs are reported in figures 6, 7, and 8. In the left figures, the symmetry is clearly visible with respect to the anti-diagonal, which is related to the mean-drift load that occurs at $f^- = f_j - f_k = 0$ resulting in a static load. With regards to figures 6, 7, and 8 (left), lines parallel to the anti-diagonals (solid black line) pertain to a given difference frequency f^-, whereas lines parallel to the main diagonals (dashed black lines) pertain to a given sum-frequency. Figures 6 and 7 show that, mainly for surge but also for pitch, the second-order wave-exciting loads are large in magnitude over a wide interval of difference frequencies, suggesting that the approximation of the second-order loads by a means of only a few off-diagonals would result in an underestimation of the overall loading for this platform. Figures 6, 7, and 8 also report (right) the difference-frequency QTF responses as a function of difference frequency. The choice of a different plotting format, with respect to the correspondent QTF loads (left), is because there are noticeable magnitudes in the response at specific frequencies (i.e., the natural frequencies, that lie near the anti-diagonals). The clearly visible peaks in figures 6, 7, and 8 are related to (respectively) the surge, pitch, and heave natural frequencies. The surge and pitch natural frequencies are visible in both figures 6 and 7 because the two DOFs are coupled.

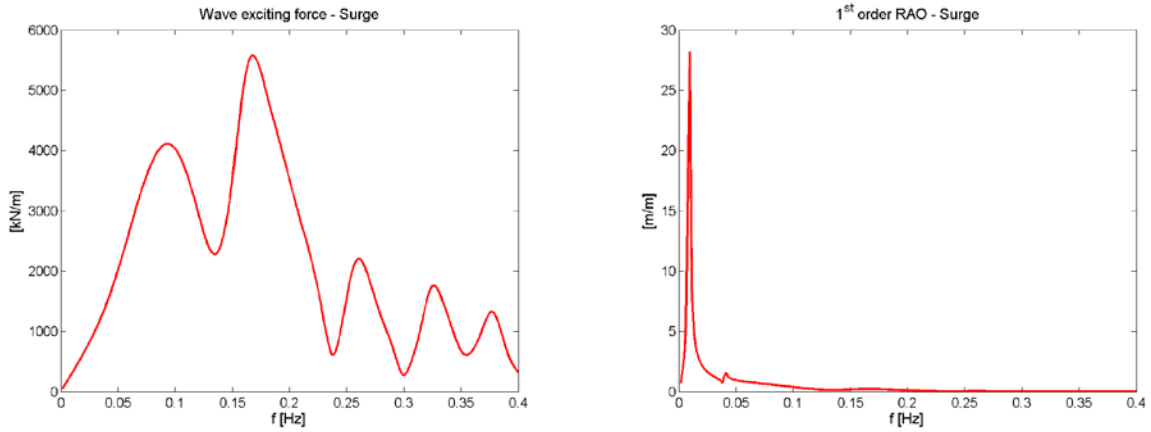

Figure 3. Surge first-order solution: wave-exciting force (left) and response magnitude (right).

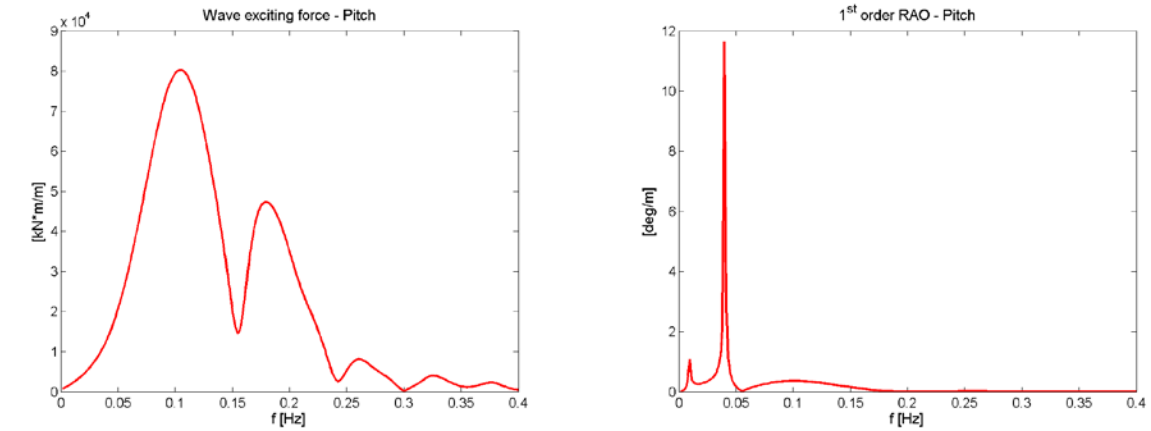

Figure 4. Pitch first-order solution: wave-exciting moment (left) and response magnitude (right).

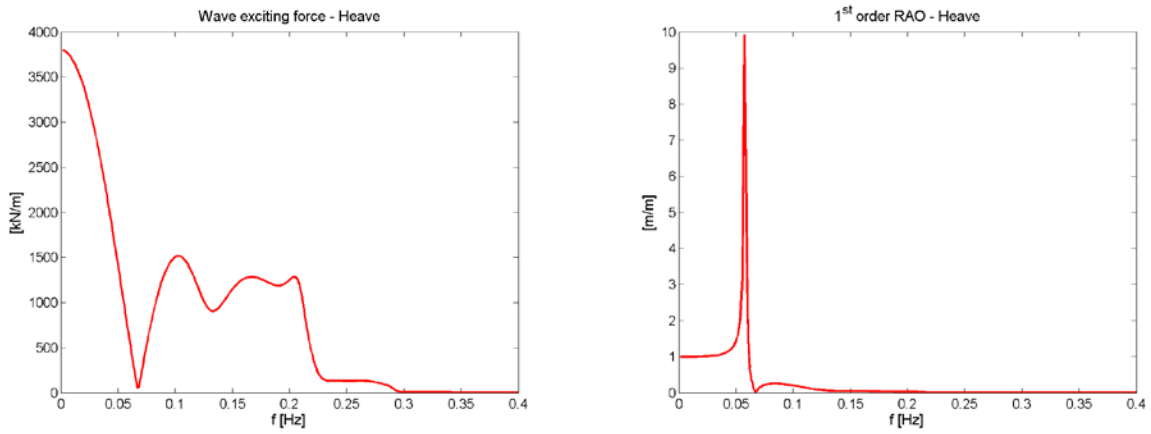

Figure 5. Heave first-order solution: wave-exciting force (left) and response magnitude (right).

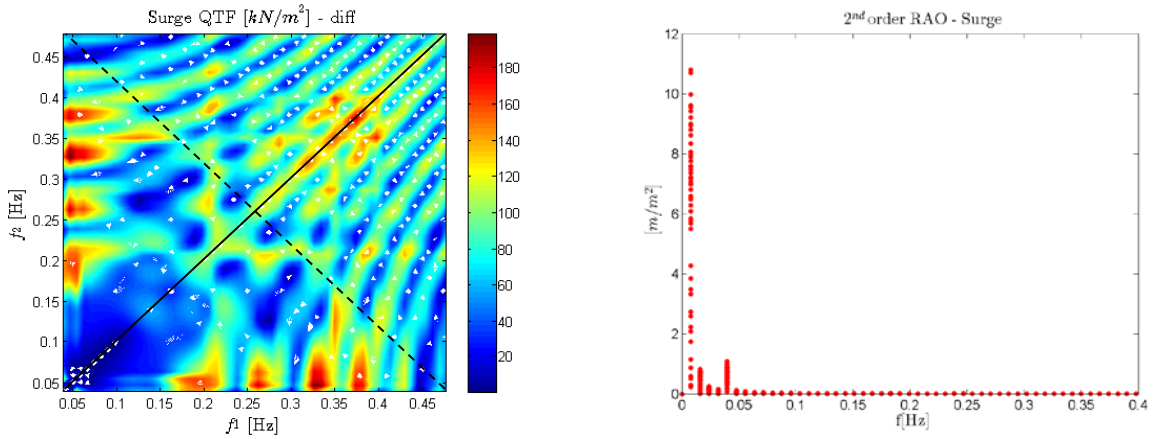

Figure 6. Difference-frequency surge: QTF force (left) and response magnitude (right).

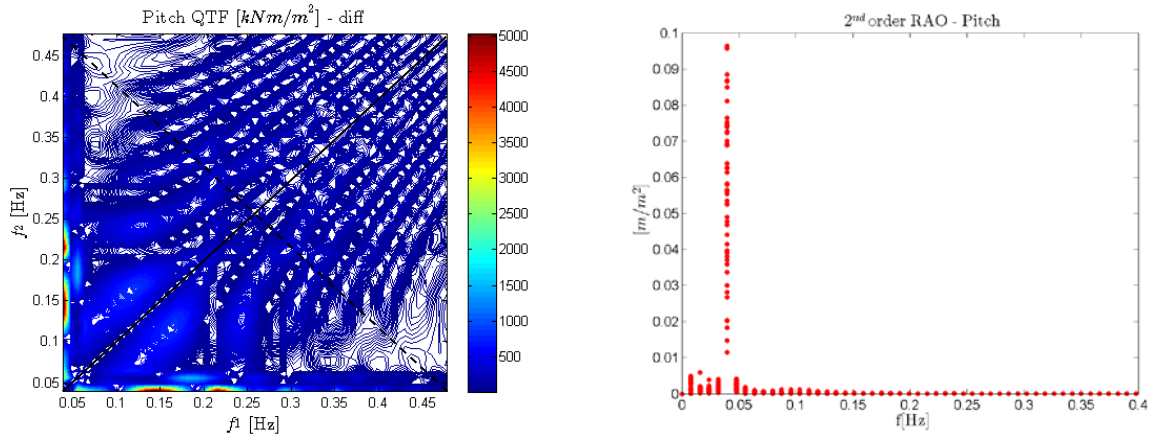

Figure 7. Difference-frequency pitch: QTF moment (left) and response (right) magnitude.

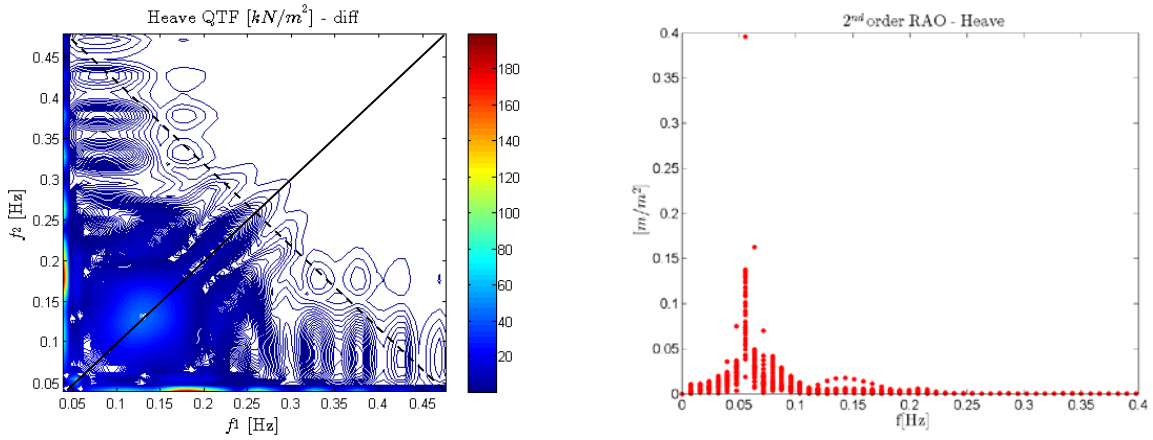

Figure 8. Difference-frequency heave QTF force (left) and response magnitude (right).

Using these RAOs and QTFs, global responses and loads were calculated for a variety of sea states. For a given sea state, different time-domain realizations lead to different global responses and loads because of the different combination of individual wave phases [4]. The sea state considered for the simulations reported herein was the JONSWAP spectrum with a significant wave height $H_s = 2\ m$ and peak-spectral period $T_p = 7.5\ s$ and the results are shown in figures 9, 10, 11, and 12 (left). The choice of sea state was based on the desire to perform future comparisons between the numerical results and the experimental data from the tests performed at the MARIN wind/wave basin, as reported in [5]. In addition, a more severe sea state ($H_s = 7\ m$ and $T_p = 10\ s$) was considered in figure 12 (right) to better demonstrate the importance of second-order hydrodynamics.

Figures 9, 10, and 11 were derived using equation (1), (2), (3), and (4). Equations (1) and (2) represent (respectively) the fast-Fourier transform (FFT) magnitudes of the first-order loads and response, whereas equations (3) and (4) represent the second-order loads and response. The wave amplitudes are related to the wave spectrum by the relation $|A(f)| = \sqrt{2S(f)df}$, where $S(f)$ is the one-sided wave spectrum and has different random phases φ_a at each frequency *f*.

$$F(f) = \left||X(f)||A(f)|e^{i(\varphi_x+\varphi_a)}\right| = |X(f)||A(f)| \tag{1}$$

$$\xi(f) = \left||RAO(f)||A(f)|e^{i(\varphi_{RAO}+\varphi_a)}\right| = |RAO(f)||A(f)| \tag{2}$$

$$F_{tot}{}^{\pm}(f_l{}^{\pm}) = \left|\sum_{f_l=f_j\pm f_k} F_{jk}{}^{\pm}A_jA_k\right| = \left|\sum_{f_l=f_j\pm f_k} \left|F_{jk}{}^{\pm}\right|\left|A_j\right||A_k|e^{i(\varphi_{jk}{}^{\pm}+\varphi_j+\varphi_k)}\right| \tag{3}$$

$$X_{tot}{}^{\pm}(f_l{}^{\pm}) = \left|\sum_{f_l=f_j\pm f_k} \xi_{jk}{}^{\pm}A_jA_k\right| = \left|\sum_{f_l=f_j\pm f_k} \left|\xi_{jk}{}^{\pm}\right|\left|A_j\right||A_k|e^{i(\varphi_{jk}{}^{\pm}+\varphi_j+\varphi_k)}\right| \tag{4}$$

In Figures 9, 10, and 11 the second-order results are reported both for loads and response and plotted along with the first-order results. What can be clearly seen from these graphs is: although the second-order loads are quite small compared to the first-order loads, particularly for the difference-frequency band, this loading results in non-negligible responses with respect to first order. This results from the excitation of system natural frequencies and a small amount of damping. The very small amount of radiation damping at these frequencies results in large resonant motion. In reality, the response will be tempered by viscous damping and potentially aerodynamic damping when the turbine is operating. Although the sum-frequency contribution is not playing an important role for the OC4-DeepCwind platform, the difference-frequency contribution is. In figures 9, 10, and 11, the results are processed by following the formulation of equations (3) and (4), and are analyzed for 15 different realizations for the given sea state. Different realizations refer to variations in the random phase $\boldsymbol{\varphi_j}$and $\boldsymbol{\varphi_k}$ for each realization. Also, the average loads and responses are reported along with the different realizations and the difference- and sum-frequency bands are shown in separate zoomed-in plots. The random phases do not impact the magnitude of the first-order loads and responses.

In figure 12, the surge DOF was chosen to compare the power spectral densities (PSDs) computed in the frequency domain from WAMIT with the PSD of the time-domain response computed in FAST. A below-rated wind speed of 9 m/s was considered for the wind/wave simulation. As previously mentioned, low-frequency wind energy is responsible for exciting the surge natural frequency at 0.01 Hz, and also the pitch natural frequency at 0.04 Hz. The PSD of the surge response was computed from FAST using the output time history, and the PSD from WAMIT was computed directly in the frequency domain using the second-order QTFs from WAMIT. The first-order PSD was computed from the first-order RAO by the canonical form of equation (5), whereas the second-order PSDs were computed by the expressions proposed in [11], reported in equations (6) and (7):

$$PSD(f) = |RAO(f)|^2 S(f) \tag{5}$$

$$S_{\xi}^{-}(f^-) = 8\int_0^{\infty} S(\mu)S(\mu+f^-)|\xi^-(\mu,\mu+f^-)|^2 d\mu \tag{6}$$

$$S_{\xi}^{+}(f^+) = 8\int_0^{\frac{1}{2}f^+} S\left(\tfrac{1}{2}f^+ + \mu\right)S\left(\tfrac{1}{2}f^+ - \mu\right)\left|\xi^+\left(\tfrac{1}{2}f^+ + \mu, \tfrac{1}{2}f^+ - \mu\right)\right|^2 d\mu \tag{7}$$

where $\boldsymbol{\xi^{-}(f_1, f_2)}$, and $\boldsymbol{\xi^{+}(f_1, f_2)}$ of equations (6) and (7) refer to the difference- and sum-frequency motion QTFs at the frequencies $\boldsymbol{f_1}$ and $\boldsymbol{f_2}$. Regarding figure 12 (left), it can be noted that the FAST wave-only results match the WAMIT first-order results quite well and in this wave-frequency range the wave loads tend to dominate, whereas wind loads tend to dominate at low frequency over second-order difference-frequency loads. This observation was already noticed in the experimental scale tests at MARIN [5], which the present results agree quite well with. Also, in the case studied in Fig. 12 (left), the relationship between wind and wave environmental loads is considered to be representative of a realistic operating condition. Figure 12 (right) has a more severe sea state and the same 9-m/s wind speed of Fig. 12 (left), where a greater influence on the natural frequency excitation from the second-order difference-frequency loads is clearly visible. The difference-frequency hydrodynamic response now exceeds the response from wind excitation.

For the floating semisubmersible type of platform, which is designed for having surge, heave, and pitch natural frequencies lower than the first-order wave spectrum frequency range, figure 12 suggests the need to calculate difference-frequency loading in FAST along with the first-order loads to gather the realistic combined effect of low-frequency wind and wave loading on the overall system dynamics, which is underestimated without considering second-order terms. The contribution of second-order sum-frequency loads are negligible for the OC4-DeepCwind platform; however, they are likely to be more important for a floating system such as a TLP [3].

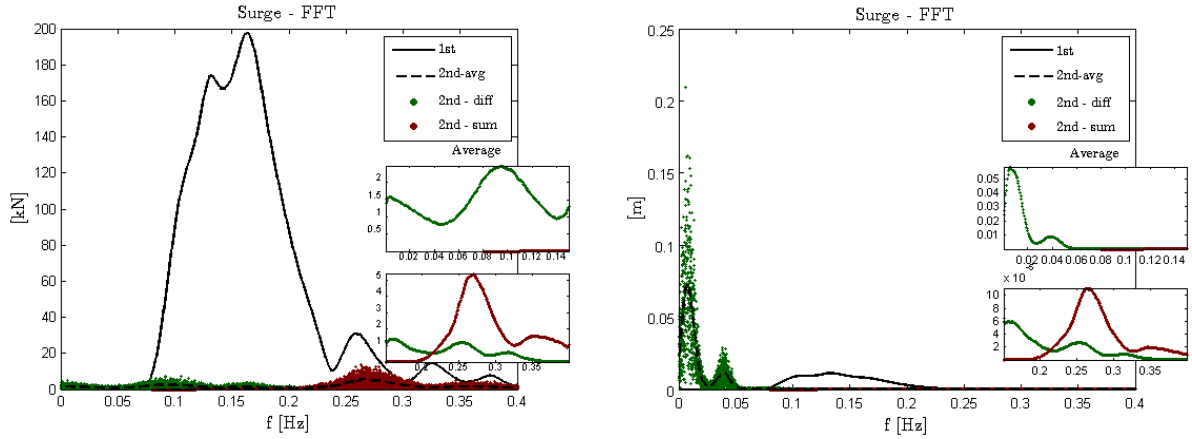

Figure 9. Fast Fourier transform magnitude of the surge hydrodynamic force (left) and surge response (right). Sea state: JONSWAP spectrum with H_s = 2 m and T_p = 7.5 s.

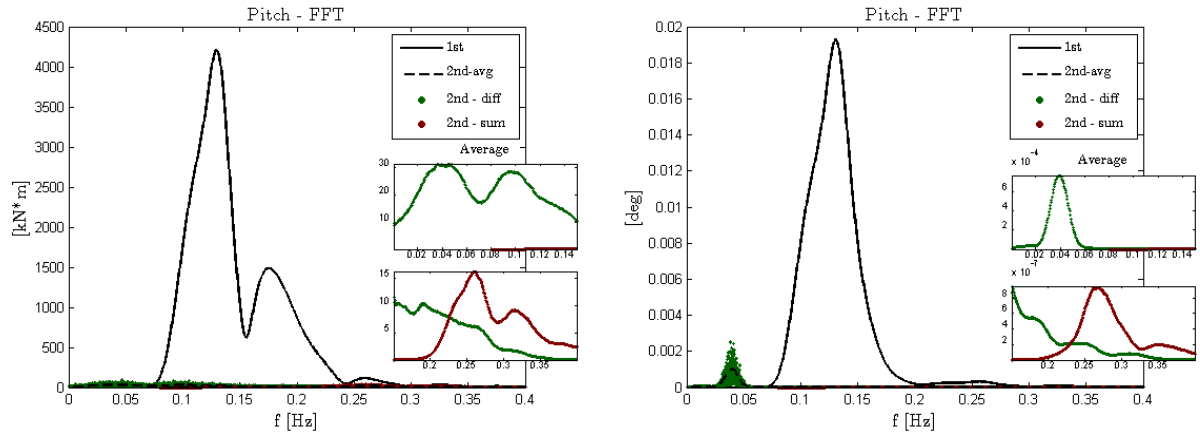

Figure 10. Fast Fourier transform magnitude of the pitch hydrodynamic moment (left) and pitch response (right). Sea state: JONSWAP spectrum with H_s = 2 m and T_p = 7.5 s.

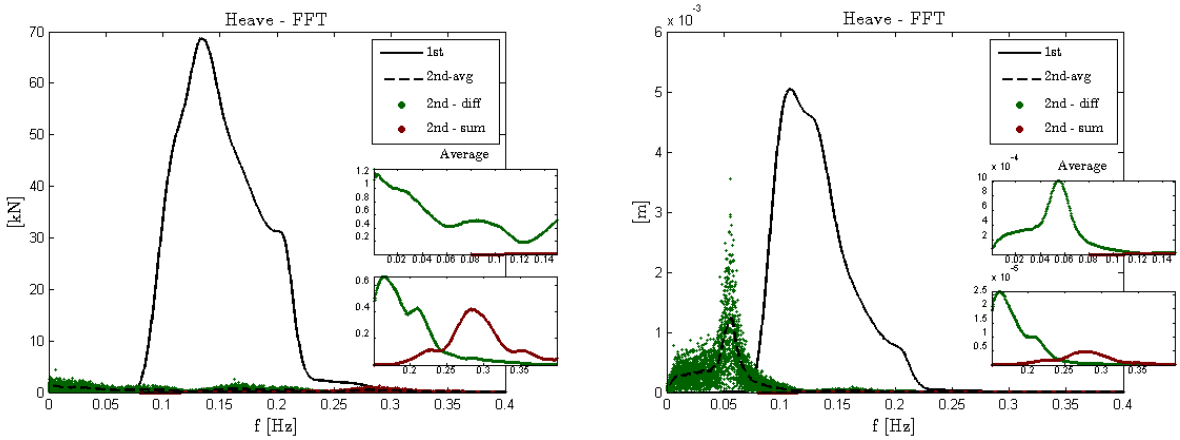

Figure 11. Fast Fourier transform magnitude of the heave hydrodynamic force (left) and heave response (right). Sea state: JONSWAP spectrum with H_s = 2 m and T_p = 7.5 s.

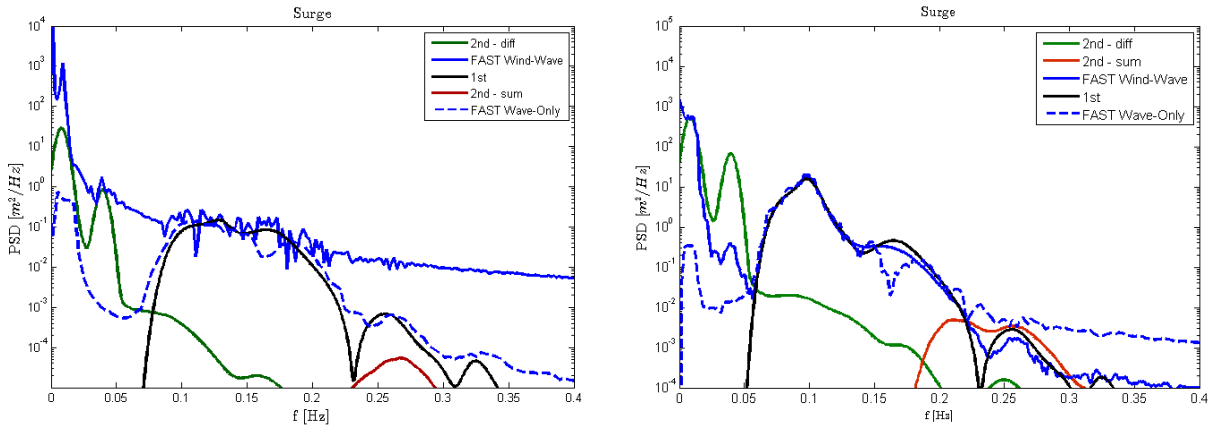

Figure 12. Surge response power spectral density comparison between WAMIT and FAST. Wind speed: 9 m/s; Sea state: JONSWAP spectrum with H_s = 2 m and T_p = 7.5 s (left), H_s = 7 m and T_p = 10 s (right).

5. Conclusions

In this paper, an assessment of the second-order hydrodynamics on a semisubmersible floating offshore wind turbine is provided. The model analyzed in this work is the Offshore Code Collaboration Continuation-DeepCwind semisubmersible and the numerical tools considered are the aero-hydro-servo-elastic computer-aided-engineering tool FAST for the turbine's time-domain modeling and the panel code WAMIT for the frequency-domain hydrodynamics. FAST is currently capable of including only first-order hydrodynamics as computed by WAMIT, and so a novel approach was taken to analyze the effects of second-order hydrodynamics without complete coupling between the two tools . The wind turbine model was "included" in WAMIT by means of mass and stiffness matrices input as external matrices to WAMIT, derived from a FAST linearization procedure. Then the first- and second-order hydrodynamics were computed in terms of difference- and sum-frequency load and response quadratic transfer functions (QTFs). A comparison between a first-order solution derived in FAST and the second-order solution from WAMIT was then carried out. The results showed that difference-frequency second-order hydrodynamics are responsible for exciting the natural frequencies of the platform, which are designed to be lower than the first-order wave spectrum frequency range. The results also agreed with the experimental data gathered from the tests performed at the Maritime Research Institute Netherlands for the same platform concept. Although WAMIT likely overestimates the response of the system because of the lack of viscous drag, it can be stated that, especially for severe sea states, the frequency content of second-order difference-frequency loads cannot be neglected in the dynamic analysis of such a system.

Future work will involve modifying FAST to import and process second-order WAMIT-load QTFs for direct time-domain analysis of floating offshore wind turbines with second-order hydrodynamic effects [12].

6. Acknowledgments

The authors would like to acknowledge DeAnna Sewell from the University of Colorado-Boulder and Line Roald from ETH Zurich for their help in providing useful advice and results important to this work. This work was supported by the U.S. Department of Energy (DOE) under Contract No. DE-AC36-08GO28308 with the National Renewable Energy Laboratory. Funding for the work was provided by the DOE Office of Energy Efficiency and Renewable Energy, Wind and Water Power Technologies Office.

References

[1] Jonkman J, Butterfield S, Musial W and Scott G 2009 *Definition of a 5-MW Reference Wind Turbine for Offshore System Development* NREL/TP-500-38060

[2] Newman J 1974 Second-order, Slowly-varying Forces on Vessels in Irregular Waves, *In Proc Symp, Dynamics of Marine Vehicles and Structures in Waves, pp. 182-6, Mechanical Engineering Publication Ltd, London*

[3] Roald L, Jonkman J, Robertson R e Chokani N 2013 The Effect of Second-Order Hydrodynamics on Floating Offshore Wind Turbines, *Proc. DeepWind*, (*Trondheim, Norway, 24–25 January 2013*)

[4] Robertson A, Jonkman J, Masciola M, Song H, Goupee A, Coulling A and Luan C (forthcoming) *Definition of the Semisubmersible Floating System for Phase II of OC4* to be published as an NREL techical report.

[5] Coulling A, Goupee A, Robertson A and Jonkman J 2013 Importance Of Second-Order Difference-Frequency Wave Diffraction Forcing In The Validation of a Fast Semi-Submersible Floating Wind Turbine Model, *Proc. 32nd International Conference on Ocean, Offshore and Arctic Engineering* (*Nantes, France, 9–14 June 2013*).

[6] Jonkman J 2007 *Dynamics Modeling and Loads Analysis of an Offshore Floating Wind Turbine* NREL/TP-500-41958

[7] Lucas J 2011 *Comparison of First and Second-Order Hydrodynamic Results for Floating Offshore Wind Structures* GL Garrad Hassan, Report Ref: 11594br02a

[8] Matha D Schlipf M Cordle A and Jonkman J 2011 Challenges in Simulation of Aerodynamics, Hydrodynamics, and Mooring-Line Dynamics of Floating Offshore Wind Turbines *Proc. 21st Offshore and Polar Engineering Conference (Maui, Hawaii, 19–24 June 2011*)

[9] Lee C H 1995 *WAMIT Theory Manual* Massachusetts Institute of Technology - Report No. 95-2

[10] Jonkman J e Buhl M 2005 *FAST User's Guide* NREL/EL-500-38230

[11] Kim M 1988 *The complete second-order diffraction and radiation solutions for a vertical axisymmetric body,* Boston: Massachussetts Institute of Techology

[12] Duarte T Sarmento A and Jonkman J 2014 *Effects of Second-Order Hydrodynamic Forces on Floating Offshore Wind Turbines*, NREL/CP-5000-60966, Golden, CO: National Renewable Energy Laboratory.